

Active Control of Type-I Edge Localized Modes with $n=1$ and $n=2$ fields on JET

Y. Liang¹, H. R. Koslowski¹, P. R. Thomas², E. Nardon³, S. Jachmich⁴, A. Alfier⁵, G. Arnoux², Y. Baranov³, M. Bécoulet², M. Beurskens³, R. Coelho⁸, Th. Eich⁶, E. De La Luna⁷, W. Fundamenski³, S. Gerasimov³, C. Giroud³, M. P. Gryaznevich³, A. Huber¹, V. Kiptily³, A. Kreter¹, L. Moreira³, V. Parail³, S. D. Pinches³, S. Saarelma³, O. Schmitz¹, and JET-EFDA contributors*

JET-EFDA, Culham Science Centre, Abingdon, OX14 3DB, UK

¹Forschungszentrum Jülich GmbH, Association EURATOM-FZ Jülich, Institut für Energieforschung - Plasmaphysik, Trilateral Euregio Cluster, D-52425 Jülich, Germany;

²Association EURATOM-CEA, 13108 St Paul-lez-Durance, France;

³EURATOM-UKAEA Fusion Association, Culham Science Centre, OX14 3DB, Abingdon, OXON, UK;

⁴Association EURATOM-Belgian State, Koninklijke Militaire School - Ecole Royale Militaire, B-1000 Brussels Belgium;

⁵Associazione EURATOM-ENEA sulla Fusione, Consorzio RFX Padova, Italy;

⁶Max-Planck-Institut für Plasmaphysik, EURATOM-Assoziation, D-85748 Garching, Germany;

⁷Asociación EURATOM-CIEMAT, Avenida Complutense 22, E-28040 Madrid, Spain;

⁸Associação EURATOM/IST, Centro de Fusão Nuclear, Instituto Superior Técnico, Av Rovisco Pais, 1049-001 Lisbon, Portugal

e-mail contact of the main author: y.liang@fz-juelich.de

Abstract. Recent experiments on JET have shown that type-I edge localized modes (ELMs) can be controlled by applying static low $n = 1$ external magnetic perturbation fields (EMPFs) produced by four external error field correction coils (EFCC) mounted far away from the plasma between the transformer limbs. When an $n = 1$ EMPF with an amplitude of a few Gauss at the plasma edge ($\rho > 0.95$) is applied during the stationary phase of a type-I ELMy H-mode plasma, the ELM frequency rises from ~ 30 Hz up to ~ 120 Hz and follows the applied perturbation field strength. The energy loss per ELM normalised to the total stored energy, $\Delta W_{\text{ELM}}/W_p$, decreased from 7 % to below the resolution limit of the diamagnetic measurement ($\sim 2\%$). Transport analysis using the TRANSP code shows no or a modest reduction of the thermal energy confinement time because of the density pump-out, but when normalised to the IPB98(y,2) scaling the confinement shows almost no reduction. Stability analysis of mitigated ELMs shows that the operational point moves from intermediate n peeling-ballooning (wide mode) boundary to low- n peeling (narrow mode) boundary with $n = 1$ perturbation fields. The first results of ELM mitigation with the $n = 2$ EMPFs on JET demonstrate that the frequency of ELM can be increased by a factor of 3.5, only limited by the available EFCC coil current. During the application of the $n = 1, 2$ EMPFs, a reduction in the ELM size (ΔW_{ELM}) and ELM peak heat fluxes on the divertor target by roughly the same factor as the increase of the ELM frequency has been observed. The reduction in heat flux is mainly due to the drop of particle flux rather than the change of the electron temperature. Similar plasma braking effect has been observed with $n = 1$ and $n = 2$ external fields when a same EFCC coil current was applied. Compensation of the density pump-out effect has been achieved by means of gas fuelling in low triangularity plasmas. An optimised fuelling rate to compensate the density pump-out effect has been identified. Active ELM control by externally applied fields offers an attractive method for next-generation tokamaks, e.g. ITER.

1. Introduction

The standard tokamak H-mode, which is foreseen as the ITER baseline operating scenario [1], is characterised by a steep plasma pressure gradient and associated increased current density at the edge transport barrier which exceeds a threshold value to drive

* See the Appendix of F. Romanelli et al., paper OV/1-2, this conference

magnetohydrodynamic (MHD) instabilities referred to as Edge Localized Modes (ELMs) [2,3]. The so-called Type-I ELMs leads to a periodic expulsion of a considerable fraction of the stored energy content onto the plasma facing components. The periodic and transient expulsion of energy onto plasma facing components is predicted to be too high and will pose a severe problem for the integrity and lifetime of these components. Melting or high erosion rates might occur under certain conditions, as it is derived from extrapolations based on present knowledge [4]. Therefore, reliable methods for the control of Type-I ELM power losses are required for operation of a future fusion machine, e.g. ITER [1].

Previous experiments on DIII-D have shown that the application of resonant magnetic perturbation fields (RMP) is a promising technique for the complete suppression of ELMs with an $n = 3$ field induced by a set of in-vessel coils [5, 6]. On JET, active control of the transient heat loads due to large type-I ELMs has been achieved with low- n ($n = 1$ and $n = 2$) fields induced by the set of EFCCs [7-9] mounted outside of the vacuum vessel [10]. When an $n = 1$ EMPF with an amplitude of a few Gauss at the plasma edge ($\rho > 0.95$) is applied during the stationary phase of a type-I ELMy H-mode plasma, the ELM frequency rises from ~ 30 Hz up to ~ 120 Hz and follows the applied perturbation field strength [7]. ELM mitigation does not depend on the orientation respect to the vacuum vessel of the applied $n = 1$ magnetic fields. Active control of type-I ELMs with $n = 1$ EMPFs has been developed for more ITER-relevant configurations and parameters in a wide operational space of plasma triangularity (δ_U up to 0.45), q_{95} (4.8 - 3.0) and beta (β_N up to 3.0) on JET [8, 11]. The results of ELM mitigation with the $n = 2$ EMPFs on JET demonstrate that the frequency of ELM can be increased by a factor of 3.5, only limited by the available EFCC coil current. A wide operational window of q_{95} has also been obtained for ELM mitigation with either $n = 1$ or $n = 2$ EMPFs [8].

2. EMPF induced by EFCCs on JET

On JET, external perturbation fields can be applied by the EFCCs [10]. The system consists of four square shaped coils (~ 6 m in dimension) which are mounted at equally spaced toroidal positions and attached to the transformer yokes as shown in figure 1(a). Each coil spans a toroidal angle of 70° and has a radial distance along the winding of 5.3 to 7 m from the axis of the machine. It has 16 turns and the maximum total coil current amounts to $I_{\text{EFCC}} = 48$ kAt. Here, the total current is given in terms of the current in one coil winding times the number of turns. Depending on the wiring of the EFCCs either $n = 1$ or $n = 2$ EMPFs can be created. In fact, the EFCCs system on JET was originally designed for compensation in both amplitude and phase of the $n = 1$ harmonic of the intrinsic error field arising from imperfections in the construction or alignment of the magnetic field coils.

Previous studies of the error field on JET show that the amplitude of the intrinsic error, $B_{n=1}^{\text{err}}(q=2)/B_0$, is only in the order of 10^{-5} [12] which corresponds to a few kAt of EFCC current. The effective radial resonance magnetic perturbations, $|b_{r,\text{eff}}^{\text{res}}| = |B_{r,\text{eff}}^{\text{res}}/B_0|$, calculated for $I_{\text{EFCC}} = 1$ kAt in both $n = 1$ and $n = 2$ configurations are shown in figure 1(left), where $B_{r,\text{eff}}^{\text{res}}$ and B_0 are the radial resonant magnetic perturbation field and the toroidal magnetic fields, respectively [8]. In the $n = 1$ EFCC configuration, the amplitude of the $n = 1$ harmonic is one or two magnitudes larger than other components ($n = 2, 3$). However, there is still an $n = 1$ harmonic existing in the $n = 2$ EFCC configuration due to the geometry of the EFCCs, and the amplitude of $b_{r,\text{eff}}(n = 1)$ is similar to that of $b_{r,\text{eff}}(n = 2)$ at the plasma edge. Although the amplitude of $b_{r,\text{eff}}(n = 2)$ in $n = 2$ EFCCs is by a factor of 3 smaller than $b_{r,\text{eff}}(n = 1)$ in $n = 1$ EFCCs, the number of resonant surfaces increased by a factor of two and the distances between resonant surfaces are reduced too.

Figure 1 (middle and right) shows also two examples of combined Poincaré and laminar plot for $n = 1$ and $n = 2$ EFCC configuration. These initial results clearly exhibit the stochastic nature of the field line behaviour. The region around the X-point is sufficiently stochastic and the lobes of the stable and unstable manifolds step out [13]. These field line trajectories caused by the combination of the resonant island chains and the divertor X-point are immanent indication of a resonant destruction of the magnetic field and by that of edge ergodisation. Here, the calculation is based upon an equilibrium reconstruction for pulse #67954 on JET with the perturbing field in vacuum superimposed. Screening effects due to plasma rotation have been neglected.

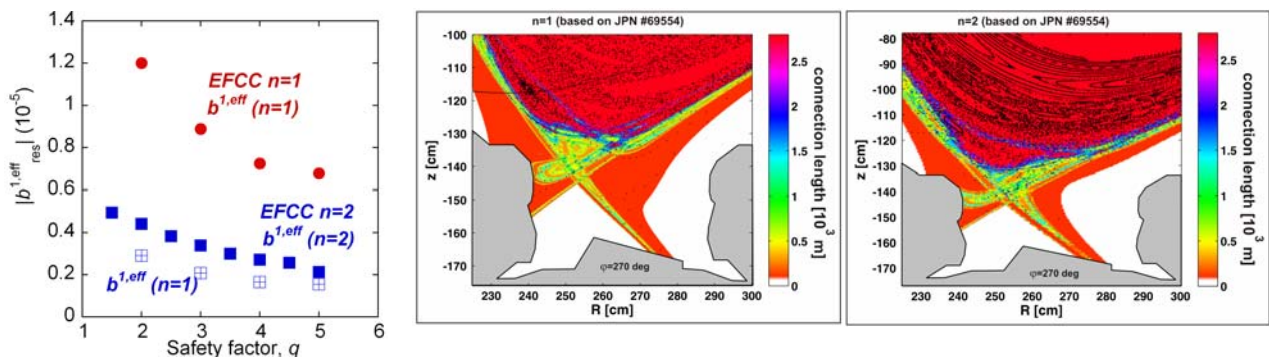


Figure 1. (left) Effective resonant magnetic perturbation for 1 kAt in the EFCCs in $n = 1$ and $n = 2$ configurations. Poincaré and laminar plot for (middle) $n = 1$ and (right) $n = 2$ EFCC configuration with $I_{EFCC}=32$ kAt.

3. Experimental results of ELM mitigation with the low n EMPF on JET

An overview on an ELM mitigation pulse is shown in figure 2. The traces are (a) the total input power, P_{tot} , and the total stored energy, E_{dia} , (b) upper and lower plasma triangularity, δ_U , δ_L , (c) I_{EFCC} , (d) the line-integrated electron densities $n_e l$, measured with an interferometer along two lines of sight, one close to the magnetic axis (upper trace) and the other near the

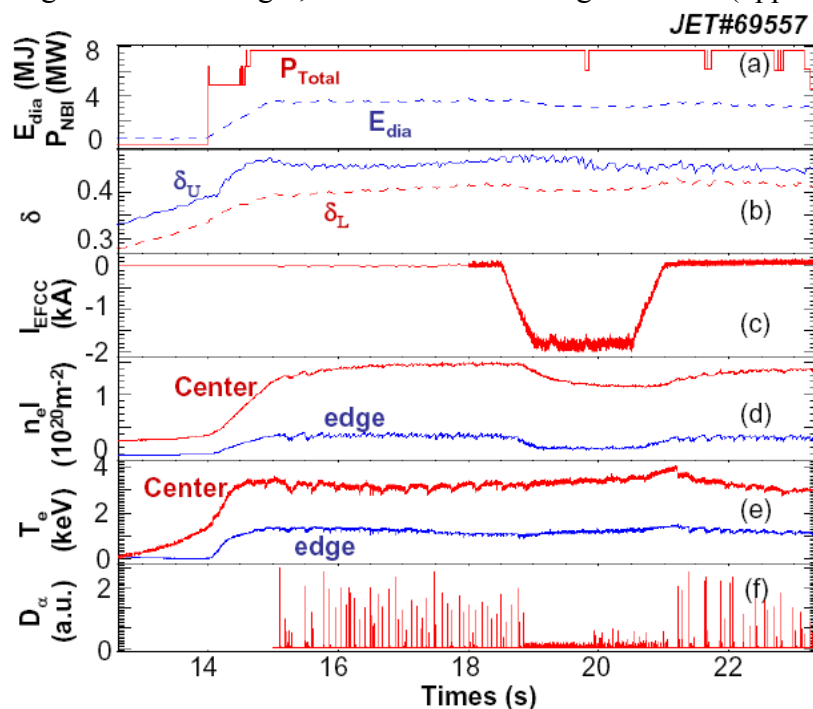


Figure 2. (a)–(f) Overview on a typical ELM mitigation experiment in a high triangularity plasma

pedestal top (lower trace) (the integration lengths of core and edge probing beams are ~ 3.2 m and ~ 1.5 m, respectively), (e) electron temperature in the core and near the pedestal top, (f) the D_α signal measured at the inner divertor. The pulse had a toroidal magnetic field of $B_t = 2.1$ T and a plasma current of $I_p = 1.8$ MA, corresponding to an edge safety factor of $q_{95} = 4.0$. In these experiments, the type-I ELMy H-mode plasma with a high triangularity shape ($\delta_U = 0.45$ and δ_L

= 0.4) was sustained by neutral beam injection (NBI) with an input power of 7.5 MW for ~ 10 s. The electron collisionality at the pedestal is ~ 0.2 . No additional gas fuelling was applied during the H-mode phase. The $n = 1$ perturbation field created by the EFCCs has a flat top with $I_{\text{EFCC}} = 32$ kAt for 2 s, which is by a factor of ~ 8 longer than the energy confinement time of this pulse. Here, the EFCC coil current is only limited due to the I^2t thermal rating limit of the power supplies. During the EFCC phase, the D_α signal (f) measuring the ELMs showed a strong reduction in amplitude. The ELM frequency increased from ~ 30 Hz to ~ 120 Hz, while the periodic energy loss due to the ELM crashes normalized to the total stored energy, $\Delta W/W$, measured by the fast diamagnetic loop, indicates a strong reduction from $\sim 8\%$ to values below the noise level ($< 2\%$) of the diagnostic. A continuous decrease in the electron density is observed in the core and edge line-integrated electron density signals even during the flat top of I_{EFCC} . A modest drop (a few per cent) in the total stored energy has been observed during the ELM mitigation phase with the EFCCs.

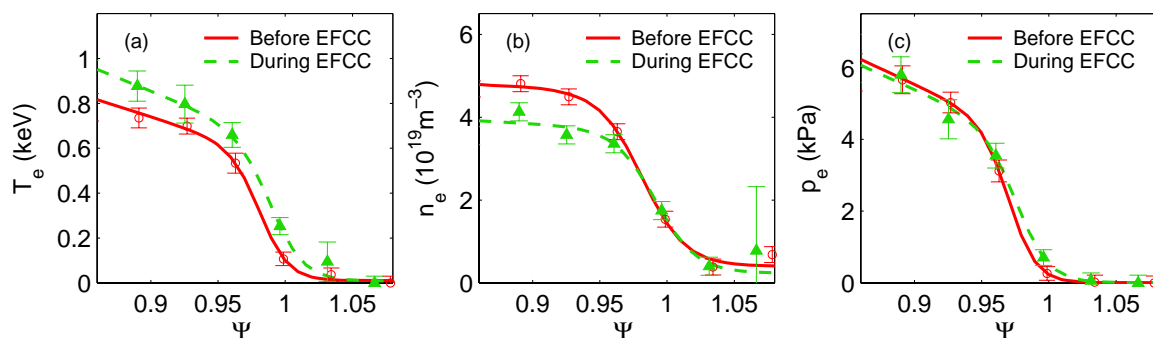


Figure 3. The radial profiles in normalized flux coordinate (Ψ) before (full line and empty circles) and during (dashed line and full triangle) mitigation.

Figure 3 shows edge profiles of (a) T_e ; (b) n_e and (c) electron pressure p_e plotted in the normalized flux coordinate measured by using the High Resolution Thomson Scattering (HRTS) diagnostic from the same discharge shown in Fig. 2 [14]. The electron density at pedestal decreases by $\sim 20\%$ due to so called density pump-out [15] during the application of the $n = 1$ EMPFs, while the pedestal electron temperature increases keep the pedestal pressure almost in constant. However, the pedestal pressure gradient obtained from the derivative of the fit shows that the maximum pressure gradient profile is decreased by 20% during the application of the $n = 1$ EMPF, and the edge pressure barrier is 20% wider: This is an effect mostly ascribable the strong decrease in n_e pedestal height with an almost unvaried width.

The stability analysis using the ELITE code shows that the ELM triggering instability is changed from intermediate- n ($n = 15$) peeling-ballooning mode (driven by both the current density and the pressure gradient) into a low- n ($n = 3$) peeling mode (driven only by the current density) [16]. The most unstable mode width decreases from 3% of the poloidal flux as the plasma crosses the stability boundary while during the edge stochasticisation, the mode width grows gradually from almost zero as the stability boundary is crossed, i.e. the modes that become unstable first, thus triggering the ELM, are very narrow ($\sim 1\%$ of the poloidal flux) in radial extent. Assuming that the width of the ELM triggering instability (i.e. the width of the most unstable mode) affects the ELM size, this could explain why the ELM size is reduced at the activation of the $n = 1$ EMPF.

Figure 4 shows the reduction factor of the peak divertor surface temperature (square) and peak heat flux (diamond) measured by an IR camera viewing the outer strike point as a function of the increases of ELM frequency with an application of the $n = 2$ EMPF [9, 17]. During the application of the $n = 2$ EMPFs, the ELM peak heat fluxes on the divertor target

reduces by a roughly the same factor as the increase of the ELM frequency. It is consistent with the reduction in the ELM size (ΔW) by the same factor. The reduction in heat flux is mainly due to the drop of particle flux rather than the change of the electron temperature. Here, the heat fluxes are measured by both Langmuir probes embedded in the divertor tiles and a fast IR camera viewing the divertor targets. A reduction in the particle flux has been also observed on the outer limiter during the ELM mitigation with EMPF as shown in Fig. 5. The normalized number of larger ELMs indicated with a larger particle flux reduced significantly which benefits the life time of the limiter.

In addition, the results from the quartz microbalance (QMB) [18] measuring the amount of carbon deposited in the inner divertor louvre indicates clearly less erosion of carbon on the divertor with mitigated ELMs. In type-I ELMy H-mode plasmas, netdeposition of carbon on the QMB with a growth rate of ~ 0.6 nm/s was observed. However, when the large ELMs were mitigated by an application of low n EMPFs, net-erosion of carbon from the QMB (~ 0.25 nm/s) was observed, which is mainly due to a strong reduction of the carbon flux but still having a significant deuterium flux.

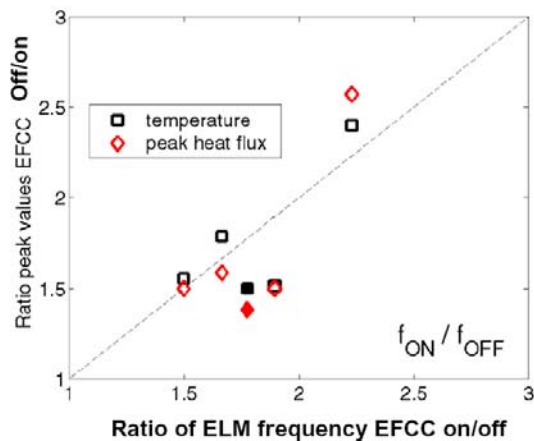


Figure 4. Heat load mitigation efficiency with an $n = 2$ EMPF

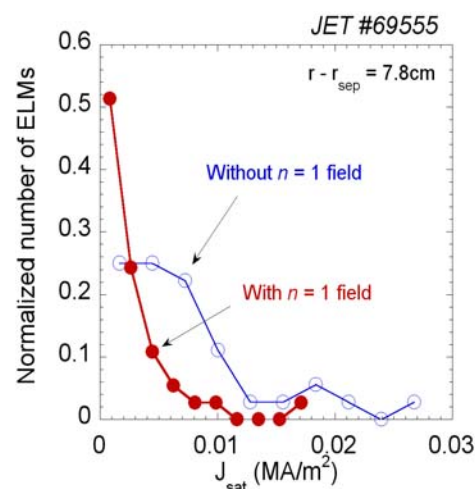


Figure 5. Normalized number of ELMs as a function of the saturation current measured during ELMs with and without an $n = 1$ EMPF.

To identify the character of the mitigated ELMs a heating power scan with four different levels of NBI power, P_{NBI} , of 10, 11.2, 14, 15.2 MW has been carried out. The target plasma was operated with ITER baseline scenario ($q_{95} = 3$) with I_p of 2 MA and B_t of 1.85 T. Figure 6 shows the ELM frequency as a function of P_{NBI} . The frequency of the mitigated ELMs increases when P_{NBI} is increased. The power dependence of the ELM frequency is similar to normal type-I ELMs (as shown in the case without $n = 1$ EMPF). However, the mitigated ELMs with $n = 1$ field have a higher frequency and are smaller in size.

Compensation of the density pump-out effect due to the application of the external $n = 1$ field has been performed with gas puffing on JET. The target plasma in this experiment is chosen from the power scan in the ITER baseline scenario described in the previous section. The gas puffing started just after the injection of NBI and ~ 1 s before the $n = 1$ field was applied. The total gas puffing rate has systematically increased from discharge to discharge from 4.2, 7.8, 11.9, up to $15.4 \cdot 10^{21}$ el/s keeping the same NBI input power of 11.2 MW.

Figure 7 shows that the central line integrated electron density as function of I_{EFCC} . Without additional gas fuelling, the electron density starts to drop at $I_{\text{EFCC}} = 13$ kAt. The reduction of $n_e l$, $\Delta n_e l$, due to the pump-out effect does linearly depend on the amplitude of I_{EFCC} . However, a contiguous drop in $n_e l$ is observed even after I_{EFCC} reached the flat top value, which indicates that full stationarity hasn't been reached in the unfuelled case. The Greenwald

fraction, f_{GW} , drops from 0.68 to 0.55. When gas puffing is applied with a total gas rate of $7.8 \cdot 10^{21}$ el/s, the target plasma density increased ($f_{\text{GW}} = 0.73$) and maintains a constant value even with application of the $n = 1$ perturbation field. The further increase of the gas fuelling rate up to $15.4 \cdot 10^{21}$ el/s yields a Greenwald density of $f_{\text{GW}} = 0.95$ before application of the $n = 1$ field, however, the plasma density drop with increasing I_{EFCC} appears again after the critical I_{EFCC} of 13 kAt was exceeded. These results demonstrate that there is an optimized fuelling rate for the compensation of the density pump-out effect. Nevertheless, the plasma confinement becomes worse when the plasma density is chosen too high (close to Greenwald Limit) in the low triangularity target plasma. There is a limitation to achieve a high plasma density without degradation of plasma confinement with an $n = 1$ field in low triangularity plasmas. Further investigation of the ELM mitigation with an $n = 1$ field will be performed in high density, high triangularity plasmas in the near future. However, it should be noted that there is no further drop of the density during the flat top of I_{EFCC} in the discharges with gas fuelling.

The influence of an $n = 1$ field on the profiles of n_e , T_e and p_e for the discharges with no gas fuelling and optimized gas fuelling at a rate of $7.8 \cdot 10^{21}$ el/s. Without gas fuelling, the application of an $n = 1$ field lets the density drop everywhere from core to edge while the electron temperature increases in the core stronger than that at the plasma edge. By application of gas fuelling, both, plasma density and temperature in the plasma core remain the same as before. However, an increase of the edge density and a drop in the edge temperature are observed. The electron density profile is getting flatter with gas fuelling, while the temperature profile becomes steeper in the plasma core. A similar influence of an $n = 1$ field on the electron pressure profile has been observed in plasmas with and without gas fuelling.

Below the optimised fuelling rate, the influence of gas fuelling on the frequency of the mitigated ELMs is weak. Once the gas rate increases over the optimised value, a clear rise of the ELM frequencies is observed in both cases with and without the $n = 1$ EMPF.

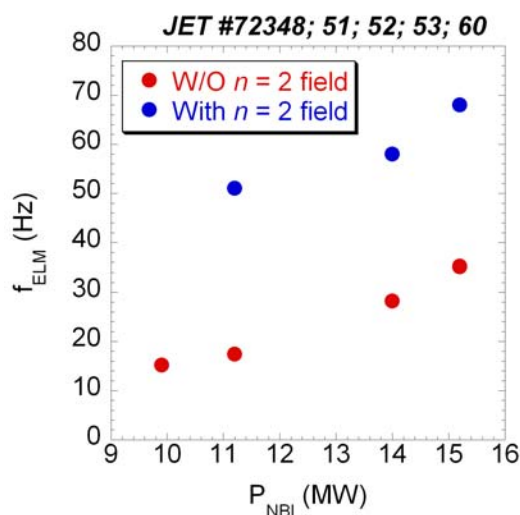


Figure 6. Heating power dependence of ELM frequency measured during the phases with and without an $n = 1$ EMPF.

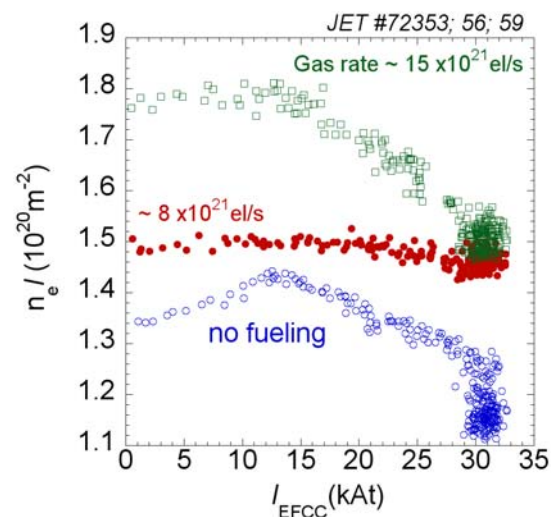


Figure 7. Central line-integrated density as a function of I_{EFCC} for the discharges with and without gas fuelling.

Self-similar braking of plasma toroidal rotation (v_{tor}) has been observed at plasma core during application of EFCC in both, $n = 1$ and $n = 2$ configurations while a strong braking appears at the plasma edge near the pedestal. Figure 8 shows the time evolutions of plasma toroidal rotation v_{tor} (upper), I_{EFCC} and (middle) the normalized toroidal ratio to that measured before application of EFCC in a target plasma ($I_p = 1.4$ MA; $B_t = 1.84$ T; $q_{95} = 4.6$;

$P_{\text{NBI}} = 10 \text{ MW}$). v_{tor} braking follows the increase of the EFCC coil current and depends linearly on the effective perturbation field. The edge braking effect near the plasma pedestal ($R = 3.69 - 3.77 \text{ m}$) is stronger than the braking in the plasma core ($R = 3.1 - 3.62 \text{ m}$). Here the R is the plasma major radius and the plasma magnetic axis is $\sim 3.04 \text{ m}$ in this discharge. No dependence on q_{95} (at constant B_t) has been observed in a wide window of $q_{95} = 4.8 - 3.0$. No clear dependence of toroidal rotation braking on the plasma collisionality has been observed in the range $\nu^* = 0.004 - 0.012$. The strong braking of core MHD rotation has also been observed by Mirnov coils. When the $n = 1$ EMPF was applied, the frequency of the sawteeth precursor mode, $f_{\text{PC}}^{\text{ST}}$ at in the plasma core was reduced from 10 to 6 kHz when the I_{EFCC} increased up to 24 kAt. There is a critical value of the I_{EFCC} observed above which the $f_{\text{PC}}^{\text{ST}}$ started to decrease. The changes of $f_{\text{PC}}^{\text{ST}}$ are linearly dependent on the amplitude of the I_{EFCC} after the critical value ($\sim 12 \text{ kAt}$) of the I_{EFCC} has been exceeded. Similar plasma braking effect has been observed with $n = 1$ and $n = 2$ EMPFs when a same EFCC coil current was applied. Since the amplitudes of both $n = 1$ and $n = 2$ harmonics in $n = 2$ EFCC configuration are by a factor of 4 smaller than that of $n = 1$ harmonic in $n = 1$ EFCC configuration as shown in figure 1 (right), this indicates that non-resonant magnetic braking could play a role in affecting the plasma rotation [19].

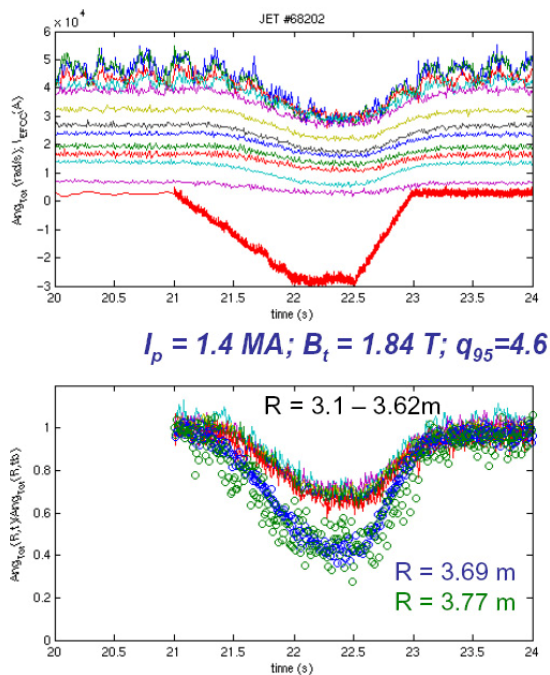


Figure 8. Time evolution of (upper) plasma toroidal angle velocity, I_{EFCC} and (lower) normalized angular frequency to that before EFCC switched on. The signals in the upper figure from up to bottom are measured from different plasma radii from core to edge.

The interaction of the $n = 2$ EMPF with the pre-seeded $m/n = 3/2$ NTM has been observed. Figure 9 shows the frequency spectrum of a Mirnov coil. The time evolution of I_{EFCC} is plotted in the same figure. The $m/n=3/2$ NTM was triggered by a large perturbation of sawtooth crash before the EFCC is applied. There is no increasing of the amplitude of the $3/2$ mode even I_{EFCC} is increased up to 32 kAt. The frequency of the $3/2$ mode reduced from 17kHz to 10kHz, while $f_{\text{PC}}^{\text{ST}}$ is reduced with a similar factor from 8kHz to 5kHz. There is no clear difference of the rotation braking effect by the $n = 2$ EMPFs for the plasmas with and without a $3/2$ NTM. This result indicates the $m/n=3/2$ sideband of the EFCC induced field

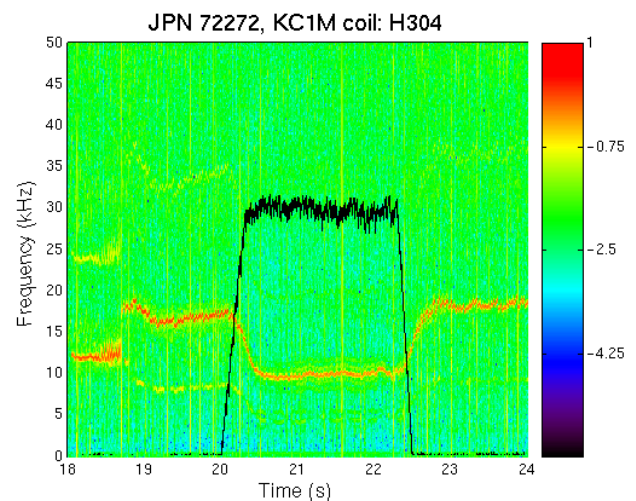


Figure 9. Frequency spectrum of a pick-up coil measurement ($I_p = 1.4 \text{ MA}$; $B_t = 1.85$; $P_{\text{NBI}} = 11 \text{ MW}$; $I_{\text{EFCC}} = 32 \text{ kAt}$).

does not penetrate deeply into the plasma core where the screening effects due to plasma rotation can not be neglected.

The $n = 1$ EMPFs has been also applied for mitigating the first ELMs after L-H transition. The preliminary results show no clear influence on the first ELMs even with the same amplitude of EFCC coil current for the mitigation of ELMs in the stationary phase.

Both, the density pump-out and the momentum braking have been also observed in the plasmas with an increased TF ripple [20]. However, the mechanisms of plasma braking are different: drag due to resonant and non-resonant magnetic braking vs counter torque due to ion losses.

4. Conclusion

In conclusions, the results of ELM mitigation with the low n ($n = 1, 2$) EMPFs on JET demonstrate that the frequency of ELM can be increased by a factor of 4, only limited by the available EFCC coil current. During the application of the $n = 1, 2$ EMPFs, a reduction in the ELM size (ΔW_{ELM}) and ELM peak heat fluxes on the divertor target by roughly the same factor as the increase of the ELM frequency has been observed. The reduction in heat flux is mainly due to the drop of particle flux rather than the change of the electron temperature. Compensation of the density pump-out effect has been achieved by means of gas fuelling in low triangularity plasmas. An optimised fuelling rate to compensate the density pump-out effect has been identified. Similar plasma braking effect has been observed with $n = 1$ and $n = 2$ external fields when a same EFCC coil current was applied. Active ELM control by externally applied fields offers an attractive method for next-generation tokamaks, e.g. ITER.

This work, supported by the European Communities under the contract of Association between EURATOM and FZJ, was carried out within the framework of the European Fusion Development Agreement. The views and opinions expressed herein do not necessarily reflect those of the European Commission.

References

- [1] ITER Physics Basis 1999 Nucl. Fusion 39 2137
- [2] Wagner F et al 1982 Phys. Rev. Lett. 49 1408
- [3] Connor J W 1998 Plasma Phys. Control. Fusion 40 531
- [4] Loarte A et al 2003 J. Nucl. Mater. 313–316 962
- [5] Evans T et al 2004 Phys. Rev. Lett. 92 235003
- [6] Evans T et al 2006 Nature Phys. 2 419
- [7] Liang Y et al 2007 Phys. Rev. Lett. 98 265004
- [8] Liang Y et al. 2007 Plasma Phys. Control. Fusion **49** B581
- [9] Liang Y et al. 2008 J. Nucl. Mater. at press
- [10] Barlow I et al 2001 Fusion Eng. Des. 58–59 189
- [11] Koslowski H R et al 2007 Proc. 34th EPS Conf. on Plasma Physics (Warsaw, Poland) P5.135
- [12] Buttery R J et al 1999 Nucl. Fusion 39 1827
- [13] O. Schmitz et al 2008 Proc. 35th EPS Conf. on Plasma Physics
- [14] A. Alfier et al Nucl. Fusion accepted for publication
- [15] Vallet J C et al 1991 Phys. Rev. Lett. 67 2662
- [16] S. Saarelma et al., 2008 submitted to Plasma Phys. Control. Fusion
- [17] Jachmich S et al 2007 Proc. 34th EPS Conf. on Plasma Physics (Warsaw, Poland) P5.099
- [18] Esser H G et al 2005 J. Nucl. Mater. 337–339 84
- [19] K.C. Shaing 2003 Phys. Plasmas 10, 1443
- [20] G Saibene et al, this conference